International Journal of Advances in Engineering and Management (IJAEM)
Volume 3, Issue 7 July 2021, pp: 3952-3963 www.ijaem.net ISSN: 2395-5252

Vehicle Warning System using Dynamic Pattern Projection with Active Mirror on Road to avoid collision between Vehicle and Pedestrians.

Mr. Ghayatadak Jaibhimrao Eknath
Student of Dept. of Computer Engineering.
Vishwabharati Academy's college of Engineering, Ahmednagar, Maharashtra, 414201, India.

Submitted: 15-07-2021 Revised: 29-07-2021 Accepted: 31-07-2021

ABSTRACT: Recently, the demand for vehicle warning systems to avoid collisions between vehicles and pedestrians has been increasingly growing. For the implementation of such systems, three types of vehicle-to-pedestrian (V2P) technologies are widely adopted. In the first, vehicles communicate with pedestrians via smart devices using dedicated short-range communications (DSRC), but it is neither simply intuitive nor fast responsive. In the second, vehicles generate a noise in order to help pedestrians avoid collisions, at the expense of disturbing others with unwelcome noise. In the last, an on-road short-range projection technique visually informs pedestrians that a vehicle is approaching, which can be more intuitive and responsive. However, the two main drawbacks of conventional on-road projections are that they involve a static pattern and narrow emission angle. This paper proposes an on-road dynamic pattern projection technique for grabbing more attention from pedestrians with various dynamic patterns and covering a wide emission angle using an active mirror. Theoretical analysis shows that the on-road projection pattern and its angle can easily be controlled by adjusting the switching frequency, duty-cycle, andamount of current flow in the control circuitry. The simulation and experimental results validate that various patterns can be projected within a projection angle of±70° at a power consumption less than 0.98W.

KEYWORDS: Vehicle warning, vehicle-to-pedestrian (V2P), on-roadprojection, dynamic pattern, active mirror.

I. INTRODUCTION

GOVERNORS highway safety association (GHSA) announced that the number of pedestrian fatalities increased from 2007 to 2016 by 27% [1]. In addition, the national highway traffic safety administration (NHTSA) reported in 2016 that there were 5,987 pedestrian fatalities in traffic crashes in the United States [2]. It is important to note that the reports by both GHSA and NHTSA indicated that 75% of pedestrian fatalities occurred in the dark. Furthermore, NHTSA reported that an average of 210 fatalities and 15,000 injuries per year are caused by back over crashes. Not-in-traffic surveillance (NiTS) system reported similarly that 284 fatalities and 12,000 injuries on average occur every year due to back over crashes [3]. Children aged five and under account for 31% of back over fatalities each year, while elderly people aged 70 and over account for 26%. In order to prevent these accidents by warning pedestrians, several vehicle-to-pedestrian (V2P) technologies have emerged. First, dedicated short-range communications (DSRCs) have been developed by forwarding warning signals to pedestrians via smart devices [4]–[6], but these are not useful for people without smart devices, particularly vulnerable road users (VRUs) such as children and elderly people who do not have a smart device or do not know how to use it. Second, a back-up beeper can be used by generating sound to warn pedestrians about an impending collision, but this can disturb people who are not the target of the beeper [7]–[9]. Unlike the other two techniques, on-road projection is intuitive and has been widely researched in application to a limited area [10]–[16]. As shown in Fig. 1, a light pattern is projected onto the road so as to warn pedestrians that a vehicle is approaching or around them. The on-road projection is a means to provide pedestrians with an intuitive sense of the vehicle, even if they are not carrying smartphones.

International Journal of Advances in Engineering and Management (IJAEM)
Volume 3, Issue 7 July 2021, pp: 3952-3963 www.ijaem.net ISSN: 2395-5252

Fig. 1. Conventional vehicle warning system using on-road short-range projection with a static pattern.

As for the implementation of the on-road projection, two methods can be used: using collimating lens or digital micro mirror devices (DMDs). Using a collimating lens requires a static patterned film [10], [11], but the light emission angle is proportioned to the size of the lens, resulting in a large volume.The other is a way to project pixel images through the digital micro-mirror device [12]–[14]. The drawbacks of this system are the limited emission angle and the usage of customized optical components that raises the cost of the system. In this paper, we propose an efficient on-road projection system which can project various dynamic patterns with a wide emission angle and doesnot require customized optics.

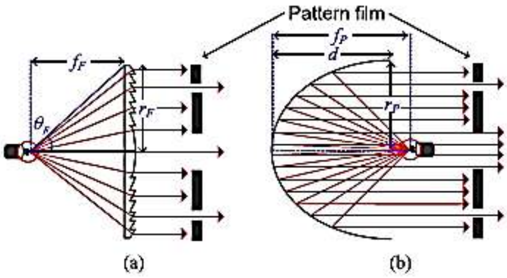

Fig. 2. Collimating lens for on-road projection (a) Fresnel lens, (b) parabolic reflector.

II. BASIC IDEA

A. Conventional Techniques

Conventional on-road projection techniques with a collimating lens, as shown in Fig. 2, are composed of a light source, a collimator, and a pattern film. Fig. 2(a) shows a system with a Fresnel lensofwhichradius rF is equal to fF tanθF , wherefF is the focal length and θF is the emission angle of the light source [11]. To have a larger pattern, larger volume cannot be avoided due to increased values of either fF or θF . The radius rP of the parabolic reflector shown in Fig. 2(b) is proportionalto the square root of fP d, where fP is the focal length and dis the depth of the parabolic reflector [12]. There are severaldrawbacks to these techniques. First, the size of the optics forcollimating light increases in order to allow for the projectedpattern to be enlarged, since the radius of the projected patternsfor both techniques is proportional to their focal length.Second,the projected light cannot be dynamically changed, resulting ina fixed pattern that may fail to attract pedestrians [10], [11].Another technique for on-road projection adopts DMDs witha projection lens [12]–[14]. While it is advantageous to have dynamic patterns that can be projected using numerous pixels,its patterns cannot be projected idely due to the fact that thetilting angle of DMDs is limited to ±15°. Moreover, the on-roadprojection with DMDs requires customized optics for thealignment of the lights reflected by the micro-mirror array, whichraises the cost of the system.

B. Proposed Technique

Fig. 3 shows the concept of the proposed dynamic on-road projectionwith an activemirror and multiple laser diodes (LDs) .The lights from the fixed LDs are reflected from the mirror andprojected onto the road. Then, various dynamic patterns can be formed by controlling the tiling angle θ of the active mirror. The proposed system is composed of two main blocks: LD and

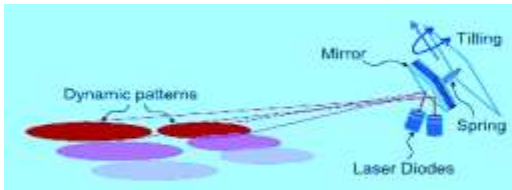

Fig. 3. Proposed dynamic on-road projection using an active mirror and multiple laser diodes.

International Journal of Advances in Engineering and Management (IJAEM)
Volume 3, Issue 7 July 2021, pp: 3952-3963 www.ijaem.net ISSN: 2395-5252

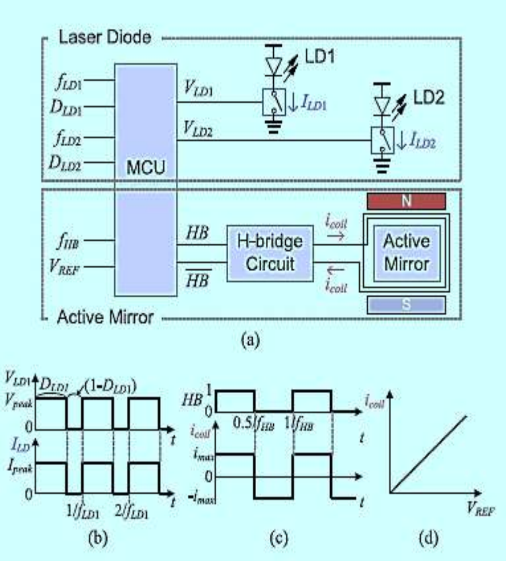

Fig. 4. Proposed system (a) block diagram, (b) timing diagram for the laser diode, (c) timing diagram for the active mirror, (d) VREF vs. icoil.

Active mirror. In the LD block, a micro-controller unit (MCU) controls the switching frequency fLD and the duty-cycle DLD of LDs, as shown in Fig. 4(a). Then, the current through the LDs, IPEAK, can be controlled as shown in Fig. 4(b). In the active mirror block, the MCU controls the switching frequency of H-bridge, fHB, with the duty-cycle of 0.5 and the current through the coil, icoil, by adjusting VREF as shown in Figs. 4(c) and 4(d). The tilting angle of the active mirror is then the function of fHB and icoil, and its relationship will be described in the next section.

The basic structure of the proposed active mirror consists of two permanent magnets, a spring, and a mirror with a coil, as shown in Fig. 5. The mirror is mounted on the fixed frame via the spring and located in between two permanent magnets with a constant magnetic field. The current through the coil and the magnetic field allows for the mirror to tilt in a given direction. If a current is supplied to the coils in one direction as shown in Fig. 6(a), Lorentz forces **FP1** and **FP2** are applied to two points **P1** and **P2** located on each side in opposing directions and let the mirror tilt in one direction by the moment. The higher number of turns in a coil or the larger the current, the larger the net current

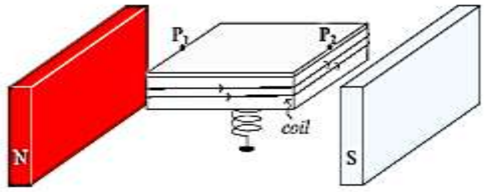

Fig. 5. Structure of the proposed active mirror.

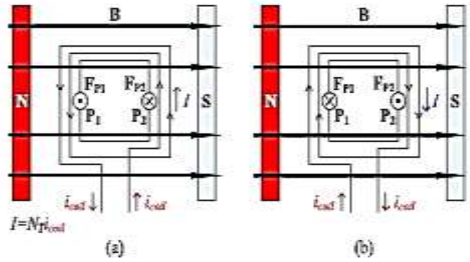

Fig. 6. Top view of the proposed active mirror. Lorentz forces applied at P1 and P2 when (a) the current in the coil flows counter-clockwise and when (b) the current in the coil flows clockwise.

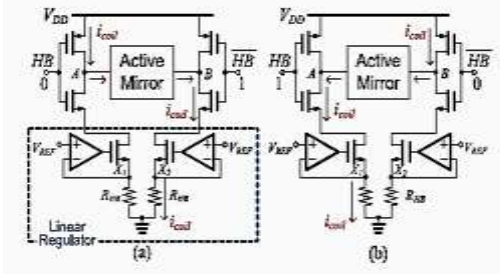

Fig. 7. Reversion of the coil current's direction depending upon whether the digital input HB is (a) low or (b) high.

I and the greater the Lorentz force **FL** is applied as

$$\mathbf{F}_L = \mathbf{F}_{P1} = -\mathbf{F}_{P2} = \mathbf{B} n i_{coil} l = \mathbf{B} I l, \qquad (1)$$

where **B** is the magnetic field, n the number of turns, icoil the current through coil, and l the length of the wire. Once the currentflowis reversed, themirror plane tilts in the opposite direction, asdepicted in Fig. 6(b) by the Lorentz forces applied in opposing directions at P1 and P2. The main advantage of the proposedactivemirror, as compared to amirror controlled by a DCmotor,is that the resilience of the spring allows for automatic alignmentof the active mirror without the need for an additional control tocheck the tilting angle of the mirror.In order to control the direction of the current through the coiland the amount of current, an H-bridge with an active mirror isproposed, as depicted in Fig. 7. Similar to the conventional Hbridgecircuits presented in [17]–[23], thecontrolHBdeterminesthe direction of the current flowing through the active mirror. IfHB is low, as shown in Fig. 7(a), the current flows from node A toB. Once HB is set to a high value, as in Fig. 7(b), the current flows from the node B to A. In addition, the amount of the current icoil can be adjusted to the desired value through the linear regulator, and can be defined as

icoil = VREF/RHB. (2)

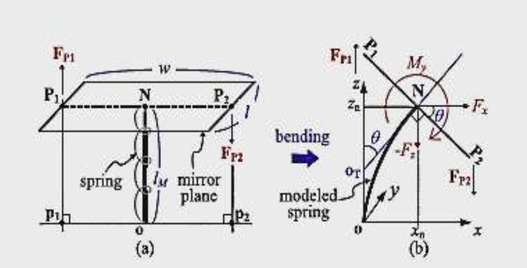

Fig. 8. Static analysis of the proposed active mirror (a) angled view of the active mirror without bending forces, (b) simplified cross-sectional view of the active mirror with bending forces.

III. MATHEMATICAL MODELING

A. Force and Moment Balance Equations

Fig. 8(a) shows an angled view of the proposed active mirror. The mirror is simplified as a plane, and the spring is an elastic bar, since the lateral buckling of a coil compression spring can be treated the same as an elastic bar [28]. The static analysis for the moment and net forces in the x-, y-, and z-axis is based on the assumption that the moment and all of the forces acting on the active mirror can be transformed to the moment and the forces at the center of the active mirror plane [24]–[27]. The mirror plane with a tilting angle θ about axis z, as shown in Fig. 8(b), can be obtained using the rotational matrix **R** from Rodrigues' formula in [24] as **R** = I + ˆ**ω** sin θ + ˆ**ω**(1 − cos θ)

$$= \begin{pmatrix} \cos\theta\ 0\ \sin\theta \\ 0\ 1\ 0 \\ \sin\theta\ 0\ \cos\theta \end{pmatrix} \qquad (3)$$

$$T= \begin{pmatrix} \cos\theta\ 0\ \sin\theta\ xn \\ 0\ 1\ 0\ 0 \\ -\sin\theta\ 0\ \cos\theta\ zn \\ 0\ 0\ 0\ 1 \end{pmatrix} \qquad (4)$$

Using the homogeneous transformation matrix in Eq. (4), as shown in Fig. 8(b), new vector coordinates of the mirror plane at location P1 and P2 after bending can be expressed as

P1 = **T** · **p1**,P2 = **T** · p2,**N** = **T** · **o**, (5)

Defining w as the width of the mirror plane, then, each position can be addressed as

p1 = [−w/2, 0, 0, 1]^T, **p2** =[w/2, 0, 0, 1]^T,
o = [0, 0, 0, 1]^T. Since the Lorentz forces acting on the active mirror are always perpendicular to the ground, they can be defined as

FP1 = [0, 0, FL]^T ,**FP2** = [0, 0,−FL]^T . (6)

where FL is the scalar of Lorentz force **FL**. Then, the moment and force balance equations of the proposed system can be

$$[M_x, M_y, M_z]^T = \overrightarrow{\mathbf{NP_1}} \times \mathbf{F_{P1}} + \overrightarrow{\mathbf{NP_2}} \times \mathbf{F_{P2}}, \qquad (7)$$

$$[F_x, F_y, F_z]^T = \mathbf{F_{P1}} + \mathbf{F_{P2}} + [0, 0, -mg]^T. \qquad (8)$$

whereMx,My,Mz and Fx, Fy, Fz are the scalar moments and forces acting on the active mirror at the center of the mirror. Then they can be obtained as

Mx = 0,My = wFL cos θ,Mx = 0,
Fx = 0, Fy = 0, Fz = −mg.(9)

B. Origin of Tilting Axis

Since the change in the length of the spring by the weight of the mirror plane is not negligible, the change in length of the spring can be obtained using Hooke's law as

Fz = −mg = −k (lO − lM) , (10)

where m is the weight of the mirror plane, k the spring constant, andlO the initial length of the spring without locating the mirror on top [24], [26]. The spring can be taken into account as a flexible bar in order to investigate the lateral buckling characteristics of the spring [24], [28]. Considering the situation shown in Fig. 8, the spring will be buckled by moment My and force −FZ. For any cross-section of the spring, the equation for its deformation can be defined as

$$EI_{sm}\frac{d^2x/dz^2}{\left[1+(dx/dz)^2\right]^{3/2}} = M_y - F_z\,(x_n - x)\,. \qquad (11)$$

where E is the elastic modulus and Ism is the second moment of inertia [24], [28]. The right-hand side is the total moment applied to a cross-section of the spring. This equation does not have an analytical solution, but the numerical solution can be obtained by calculating elliptic integrals [29]. For small deflection, Eq. (11) can be linearized as

$$EI_{sm}\frac{d^2x}{dz^2} = M_y - F_z\,(x_n - x)\,. \qquad (12)$$

The two initial conditions for two functions x(z) and dx/dz for z = 0 are x(0) = 0 and dx/dz = 0, which leads to the solution as

$$x = -\frac{M_y - F_z x_n}{F_z}\left[1 - \cos\left(\sqrt{\frac{-F_z}{EI_{sm}}}z\right)\right]. \quad (13)$$

Then, the tangent equation at $z = z_n$ becomes

$$x = -\frac{M_y - F_z x_n}{F_z}\sqrt{\frac{-F_z}{EI_{sm}}}\sin\left(\sqrt{\frac{-F_z}{EI_{sm}}}z_n\right)(z - z_n)$$
$$-\frac{M_y - F_z x_n}{F_z}\left[1 - \cos\left(\sqrt{\frac{-F_z}{EI_{sm}}}z_n\right)\right]. \quad (14)$$

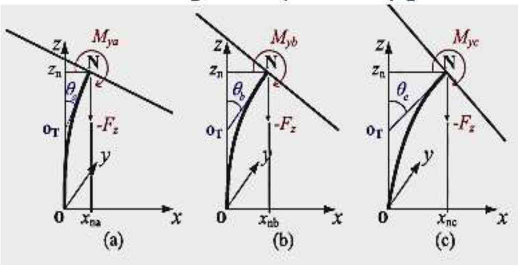

Fig. 9. Change in θ depending on different values of momentMy (a)My =Mya, (b) My = Myb, (c) My = Myc, where Mya < Myb < Myc.

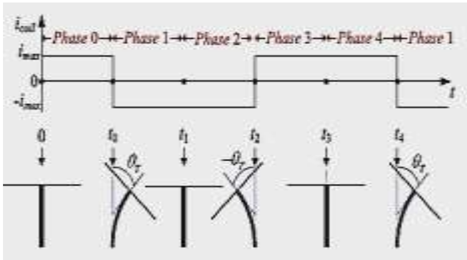

Fig. 10. Movement of the proposed active mirror depending on time.

Letting the crossing point between the tangent line and z-axis be the point **oT**, then the line between origin **o** and **oT** can be obtained as

$$\overline{oo_T} = z_n - \frac{\left[1 - \cos\left(\sqrt{-F_z/EI_{sm}}z_n\right)\right]}{\sqrt{-F_z/EI_{sm}}\sin\left(\sqrt{-F_z/EI_{sm}}z_n\right)}. \quad (15)$$

Since the line length is a constant regardless of the moment as shown in Fig. 9, the tilting angle θ becomes θ = ∠noT zn. Thus, **oT** can be defined as the origin of the tilting axis.

C. Movement of the Active Mirror

Fig. 10 describes the movement of the proposed active mirrordepending on time. There are five different phases, and afterphase 0, phases 1 to 4 are repeated periodically. The phase 0is the initial phase with which to set the target tilting angle θT ,

where the initial velocity of the active mirror is zero. In bothphases 1 and 3, θ returns to 0° from |θT | after t1−t0 = t3−t2with the non-zero initial velocity of the mirror. Similarly, inphases 2 and 4, θ becomes |θT | after some time t2−t1 = t4−t3.The operation mechanism of the proposed active mirror for theangle of ±θT is as follows. In phase 0, the current through thecoil, icoil, is applied at t=0. At the beginning of phase 1 (t=t0),the current through the coil becomes −icoil and keeps its valuethroughout the phase. Then, the direction of the current through the coil reverses every t = t0 + nN(t2 − t0), where nN is thenatural number. Thus, the active mirror tilts periodically whilemaintaining the tilting angle of ±θT , as shown in Fig. 10. As aresult, the switching frequency of the H-bridge is determined as

$$f_{HB} = \frac{1}{2(t_2 - t_0)} = \frac{1}{t_4 - t_0}. \quad (16)$$

TABLE I
TERMS USED IN KINETIC DIAGRAMS

Symbol	QUANTITY	Symbol	QUANTITY
FL	Lorentz force	kb	lateral bending stiffness
B	magnetic flux density	0	tilting angle of mirror
n	turns of coil	Im	moment of inertia
Ícoil	current flowing in a wire	Mr	moment by Lorentz force
I	product of n and Ìcoil	Mc	moment by gravity
/	length of wire receiving	Mk	moment by spring's resilience

	Lorentz force		
m	mass of moving plate	Maet	net moment of active mirror
g	acceleration of gravity		

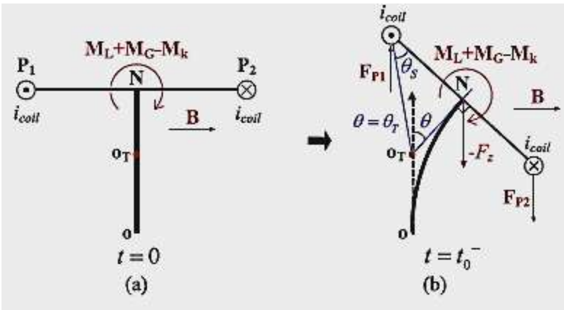

Fig. 11. Movement of the active mirror from the time (a) t = 0 to (b) t = t0-.

where t1−t0 = t3−t2 and t2–t1 = t4–t3. In order to obtain fHB, dynamic analysis of the active mirror is required. The dynamic analysis for each phase based on the parameters in Table I is as follows.

1) Phase 0: Lorentz forces are applied to both sides of the mirror plane with the current icoil to the coil at the range of 0 ≤ t ≤ t0 as shown in Fig. 11. Then moments **MP1** and **MP2** at point **oT** by Lorentz forces **FP1** and **FP2**, respectively, can be defined as

$$\mathbf{M_{P1}} = \overrightarrow{\mathbf{o_T P_1}} \times \mathbf{F_{P1}}$$
$$= \left[0, \frac{w}{2} \sec\theta_s F_L \sin(90^\circ - \theta_s - \theta), 0\right], \qquad (17)$$
$$\mathbf{M_{P2}} = \overrightarrow{\mathbf{o_T P_2}} \times \mathbf{F_{P2}}$$
$$= \left[0, \frac{w}{2} \sec\theta_s F_L \sin(90^\circ - \theta_s - \theta), 0\right]. \qquad (18)$$

By the superposition of the moments at point **oT**,**ML**, all of the Lorentz forces can be expressed as

ML = **MP1** +**MP2** = [0, wFLcos θ, 0], (19)

Since the scalar quantity of the y-axis component is positive,the tilting of the mirror plane is in a clockwise direction. Another moment at point **oT** by the gravity and the mass of mirror,**MG**, is given by

$$\mathbf{M_G} = \overrightarrow{\mathbf{o_T N}} \times (-\mathbf{F_z}) = [0, r_n mg\sin\theta, 0]. \qquad (20)$$

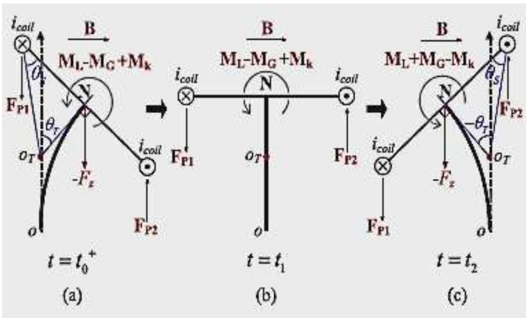

Fig. 12. Movement of the active mirror from (a) t0 + to (b) t1 and to (c) t2.

where rN is the distance between points **oT** and **N**. In addition, the moment at point **oT** by spring resilience, **Mk**, can be expressed as

MK = [0, kbθ, 0]. (21)

Since all of the moments consist only of y-axis components, the net scalar moment Mnet at point **oT** is the sum of all of the scalar moments applied at **oT** ,

Mnet = wFLcosθ + rnmgsinθ − kbθ. (22)

Mnet is also the product of the scalar moment of inertia Imand angular acceleration, which can be expressed as

$$M_{net} = I_m \frac{d^2\theta}{dt^2} = wF_L\cos\theta + r_n mg\sin\theta - k_b\theta \qquad (23)$$

However, Eq. (23) is the second-order nonlinear ordinary differential equation without an analytical solution. Assuming that sinθ≈θ and cosθ≈1 for small θ, it can be rewritten as

$$I_m \frac{d^2\theta}{dt^2} = wF_L + r_n mg\theta - k_b\theta. \qquad (24)$$

This can also be rewritten as

$$\frac{d^2\theta}{dt^2} + p\theta = q, \qquad (25)$$

where p = (kb − rNmg)/Im and q = wFL/Im. From the initial conditions θ(0)=0 and dθ/dt|t = 0, the solution for Eq. (25) can be obtained as

$$\theta(t) = \frac{q}{p}[1 - \cos(\sqrt{p}t)]. \qquad (26)$$

Thus, time tin phase 0 is dependent on angle θ and can be represented as

$$t(\theta) = \frac{1}{\sqrt{p}}\cos^{-1}\left(1 - \frac{p}{q}\theta\right). \qquad (27)$$

By setting θ = θT , the time at the target tilting in phase 0, t0, can be obtained as

$$t_0 = t(\theta_T) = \frac{1}{\sqrt{p}}\cos^{-1}\left(1 - \frac{p}{q}\theta_T\right) \qquad (28)$$

2) Phase 1: Once the direction of the current is reversed at t0, the Lorentz force is applied to the opposite direction for therange of t0 ≤ t ≤ t1, as shown in Fig. 12. Then, the tilting of the mirror plane is in a counter-clockwise direction. Thus, the netscalar moment Mnet at point oT can be expressed as

Mnet = −wFLcosθ + rnmgsinθ − kbθ. (29)

For a small θ, similar to Eq. (4), it can be approximated that

$$I_m\frac{d^2\theta}{dt^2} = -wF_L + r_n mg\theta - k_b\theta. \qquad (30)$$

It can also be rewritten as

$$\frac{d^2\theta}{dt^2} + p\theta = -q. \qquad (31)$$

From the boundary conditions θ(t0) = θT and dθ/dt|t = t0 =0, the solution for Eq. (31) can be obtained as

$$\theta(t) = (q/p + \theta_T)^{\circ}\cos(\sqrt{p}(t - t_0)) - q/p. \qquad (32)$$

The solution t = t1 for making θ(t1) = 0 can be obtained as

$$t_1 = t_0 + \frac{1}{\sqrt{p}}\cos^{-1}\left(\frac{q/p}{q/p + \theta_T}\right). \qquad (33)$$

3) Phase 2: The mirror plane is tilted counter-clockwise through the range of t1 ≤ t ≤ t2 during phase 2, as shown in Fig. 12, which leads to the net scalar moment equation Mnet at point oT becomes

$$M_{net} = -wF_L\cos\theta - r_n mg\sin\theta + k_b\theta. \qquad (34)$$

For a small θ, similar to Eq. (24), it can be approximated that

$$I_m\frac{d^2\theta}{dt^2} = -wF_L - r_n mg\theta + k_b\theta. \qquad (35)$$

It can also be rewritten as

$$\frac{d^2\theta}{dt^2} - p\theta = -q. \qquad (36)$$

In order to obtain the boundary conditions at t = t1, it is required to find dθ/dt|t=t1 from Eq. (32) as

$$\left.\frac{d\theta}{dt}\right|_{t=t_1} = -\sqrt{p}(q/p + \theta_T)^{\circ}\sin(\sqrt{p}(t - t_0)) = v_{t1}. \qquad (37)$$

By using the obtained boundary conditions dθ/dt|t=t1 = vt1 and θ(t1) = 0 , the solution for Eq. (36) can be obtained as

$$\theta(t) = \left[\frac{q}{p}\cos(\sqrt{p}(t - t_1)) - 1\right] + \frac{v_{t1}}{\sqrt{p}}\sin(\sqrt{p}(t - t_1)) \qquad (38)$$

By setting t = t2 and θ(t2) = −θT , t2 can be obtained.

According to Eq. (16), the target tilting angle ±θT can be controlled by adjusting times t0 and t2. Once time t0 is specified for target angle θT from Eq. (27), then the time t2−t0 for keeping the tilting angle at ±θT can also be determined from Eqs. (33) and (38). Note that the emission angle of the proposed on-road projection can simply be controlled by adjusting the timing for switching the direction of the current through the coil. Fig. 13 shows the emission angle by the law of reflection. Since the incidence angle is equal to the reflection angle, if the active mirror rapidly tilts from −θT to +θT , the emission angle of an on-road projection covers ±2θT . Thus, the emission angle θE of the proposed on-road projection can be defined as

|θE| = |2θT | . (39)

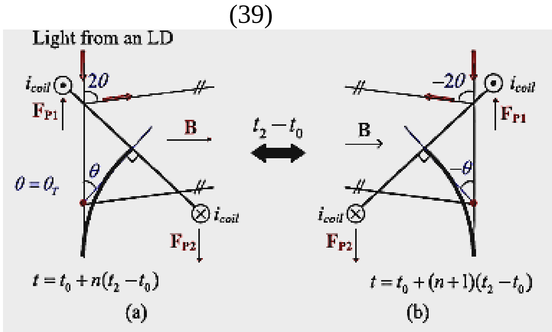

Fig. 13. Projected angle depending on the law on the law of reflection at the time (a) t0 + n(t2–t0) and (b) t0 + (n + 1)(t2–t0).

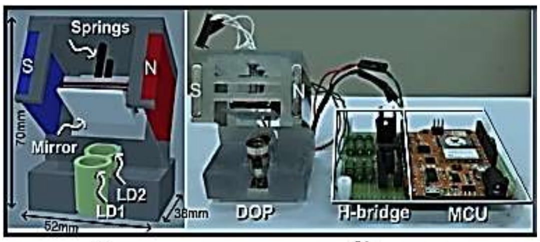

(a) (b)

Fig. 14. (a) 3D rendering of the proposed active mirror and (b) the implementation of the proposed dynamic on-road projection system.

International Journal of Advances in Engineering and Management (IJAEM)
Volume 3, Issue 7 July 2021, pp: 3952-3963 www.ijaem.net ISSN: 2395-5252

on-road projection covers $\pm 2\theta T$. Thus, the emission angle θE of the proposed on-road projection can be defined as

$$|\theta E| = |2\theta T| . \qquad (39)$$

IV. SIMULATION AND EXPERIMENTAL RESULTS

The 3Drendering of the proposed active mirror for the on-road projection technique is shown in Fig. 14(a). The two springs connecting the active mirror with the main base are used to allow the active mirror to tilt without pitch and yaw. Table II shows the design parameters used to obtain the center of the tilting axis, oT , as discussed in the lateral buckling equations for the spring. From the calculations in Eqs. (10) and (15), the length loT from the origin o to oT is 6.17mm. The design parameters for the dynamic analysis are shown in Table II as well. The prototype of the proposed dynamic on-road projection system is shown in Fig. 14(b). Fig. 15 shows the experimental results of the H-bridge in the proposed system. For the current controlling voltage VREF = 0.6 V, the maximum value of icoil is regulated to 200mAatRHB = 3 Ω. The switching frequency is purely controlled by the inputHB,where fHB = 7.5 Hz in this case. The comparisons between the simulation and experimental results for icoil depending on VREF are shown in Fig. 16. ForRHB = 2.99 Ω, the maximum error from the simulation results is less than 2.17%.

Fig. 17 compares the simulation and experimental results of the emission angle θE as adjusted by both fHB and icoil based on Eqs. (16), (27), (33), (38), and (39). θE over fHB is represented as a nonlinear graph, since θE is a sinusoidal function from Eq.

TABLE II
DESIGN PARAMETER FOR PROTOTYPE OF THE PROPOSED SYSTEM

Symbol	QUANTITY	Value
k	spring constant	154.35 N/m
l_s	length of spring	15 mm
m	mass of mirror plane	5 g
g	acceleration of gravity	9.81 m/s²
E	elastic modulus	0.24 MPa
I_{sm}*	2nd moment of inertia of 2 springs	27.4 pm⁴
l_{oT}	length of line from o to o_T	6.17 mm
n	turns of coil	45
l	wire length affected by Lorentz force	8 mm
w	width of the mirror	24 mm
d	thickness of mirror plane	9 mm
r_N	length between points N and o_T	13.33 mm
k_b	lateral bending stiffness of 2 springs	1050 μN·m/rad
I_m**	moment of inertia of mirror plane	0.99 μkg·m²

* I_{sm} is approximated as a type of a rectangular hollow section.
** I_m is approximated as a type of a annular cylinder about axis [30].

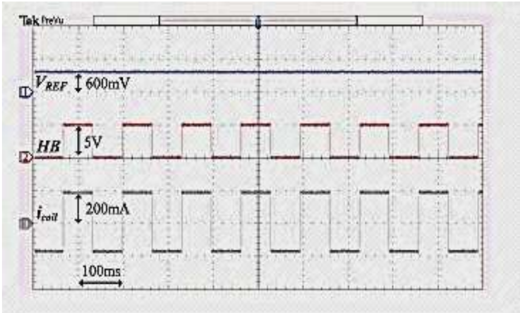

Fig. 15. Experimental results of the H-bridge at fHB = 7.5 Hz.

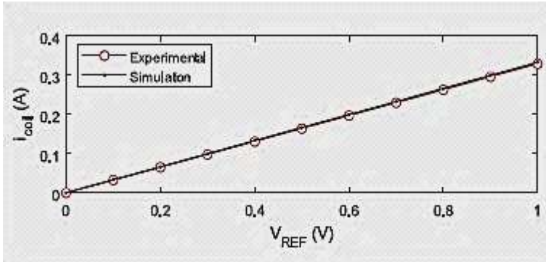

Fig. 16. Experimental results of H-bridge circuit for VREF vs. icoil.

(26) and the switching frequency fHB = 0.5(t − t2)−1 depends on t0. θE for the ranges of 5.75 Hz ≤ fHB ≤ 8.50 Hz and 70 mA ≤ icoil ≤ 200 mA are given by 4.28o ≤ |θE| ≤ 38.72 degree and 3.75 degree ≤ |θE| ≤ 60.51 degree , respectively. The mismatch of θE between the simulation and experimental results is caused by several reasons: First, in order to determine the solution of θ in terms of time in Eqs. (24), (30), it is assumed that the tilting angle of the mirror is small. Therefore, the larger the tilting angle of the mirror, the larger the error that is introduced. Secondly, the magnetic flux density B within two magnets is assumed to be a

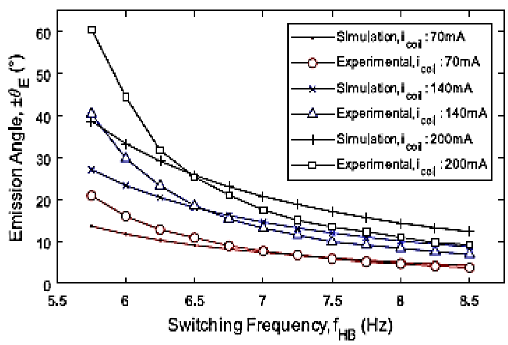

Fig. 17. Comparison between the simulation and experimental results for emission angle θE depending on various values of fHB and icoil at B =95 mT.

International Journal of Advances in Engineering and Management (IJAEM)
Volume 3, Issue 7 July 2021, pp: 3952-3963 www.ijaem.net ISSN: 2395-5252

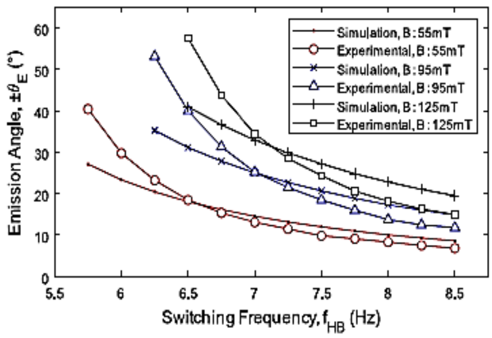

Fig. 18. Comparison between the simulation and experimental results for emission angle θE depending on various values of fHB and B at icoil = 140 mA.

constant, but it depends on the location, which can be defined as

B = μomD/2πr3 (40)

where μo is a constant known as the permeability of free space, mD is the magnetic moment of a magnetic dipole, and r is the distance from the magnetic dipole [31]. When the active mirror tilts in one direction, one side of the mirror moves close to a magnet while the other side moves away from the othermagnet. Thus, the side of the active mirror closer to the magnet is influenced by a stronger magnetic flux than the other side, which leads to the total moment by Lorentz force becoming larger as the tilting angle increases. Finally, the non-linearity of the spring constant leads to errors. The spring usually has a different spring constant depending on the angle of tilting. Fig. 18 compares the simulation and experimental results of emission angle θE adjusted by both fHB and B. Similar to Fig. 17, error between the simulation and experimental results is introduced. The error can be reduced by using a lookup table or a compensation method. Fig. 19 shows the top view of various patterns of the proposed dynamic on-road projection. The prototype is mounted 80 cm above the ground in order to mimic the position of a tail light. The on-road projected patterns are 2.5 m and 4.1 m tall for laser diodes 1 (LD1) and 2 (LD2), respectively. The emission angle

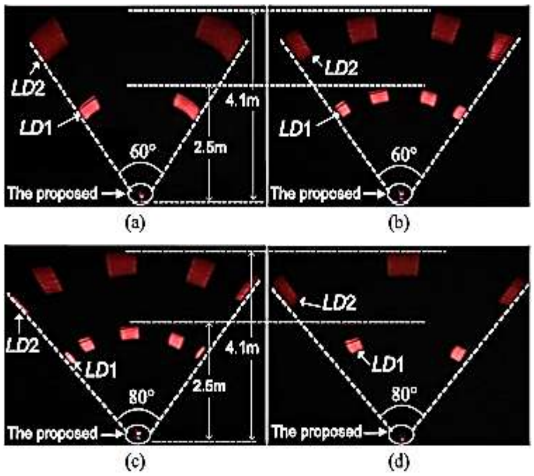

Fig. 19. On-road projection with various dynamic patterns by controlling the inputs fLD1, DLD1, fLD2, DLD2 and fHB. (a) fLD1 = 12 Hz, DLD1 = 0.5, fLD2 = 12 Hz, DLD2 = 0.5, fHB = 6 Hz, (b) fLD1 = 36 Hz, DLD1 = 0.5, fLD2 = 36 Hz, DLD2 = 0.5, fHB = 6 Hz, (c) fLD1 = 46 Hz, DLD1 = 0.4, fLD2 = 46 Hz, DLD2 = 0.4, fHB = 5.75 Hz, (d) fLD1 = 15 Hz, DLD1 = 0.15, fLD2 =23 Hz, DLD2 = 0.25, fHB = 5.75 Hz.

With the range of 3.75o ≤ |θE| ≤ 60.51o generates patterns with widths from 0.53mto 7.14m, which easily covers the full width of any vehicle. Fig. 19(a) shows the dynamic pattern with |θE| = 30◦ at fLD1 = 12 Hz, DLD1 = 0.5, fLD2 = 12 Hz, DLD2 = 0.5, and fHB = 6 Hz. If the switching frequency of each laser diode is increased while the rest of the parameters are unchanged, the projected pattern can be divided into more pieces, as shown in Fig. 19(b), where fLD1 = 36 Hz and fLD2 = 36 Hz. As shown in Fig. 19(c), the switching frequency of each laser diode is further increased to fLD1 = fLD2 = 46 Hz in order to make more pieces in the pattern. The duty-cycle of both laser diodes, DLD1 = DLD2 = 0.4, determines the ratio of light and dark patterns. |θE| = 40◦ is achieved by setting fHB = 5.75 Hz. Different patterns for LD1 and LD2 can also be formed without changing the emission angle by adjusting fLD1 = 15 Hz,DLD1 = 0.15, fLD2 = 23 Hz, and DLD2 = 0.25, as shown in Fig. 19(d). The specifications of the proposed system are as follows: VDD = 3.5 V, icoil = 140 mA, and B = 55 mT. The two VCSEL diodes have the specifications of VLD = 2.2 V,
iLD1 = 18 mA, and iLD2 = 18 mA. The horizontal and vertical emission angles are±2.86 degree and±4.76 degree, respectively. The power consumption of the proposed system, excluding the MCU, is 0.98W. Comparisons with other possible on-road projections in Table III show that the proposed technique is superior to others by

International Journal of Advances in Engineering and Management (IJAEM)
Volume 3, Issue 7 July 2021, pp: 3952-3963 www.ijaem.net ISSN: 2395-5252

generating a dynamic pattern in wide angle without requiring
expensive and bulky customized optics.

V. DYNAMIC ON-ROAD PROJECTION WITH A ULTRASONIC SENSOR

The dynamic pattern of the proposed on-road projection is controlled in conjunction with a conventional ultrasonic sensor

TABLE III
COMPARISONS WITH OTHER TECHNIQUES

	COLLIMATING LENS [11]	DMDs [13]	This work
Dynamic pattern	X	O	O
Customized Optics-free	X	X	O
Projected Angle	±20°	±39°	±70°

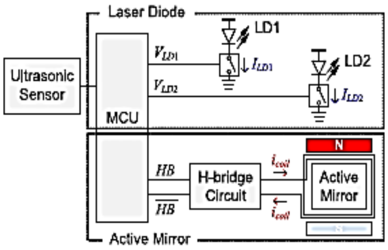

Fig. 20. Block diagram of the proposed on-road projection system with an ultrasonic sensor.

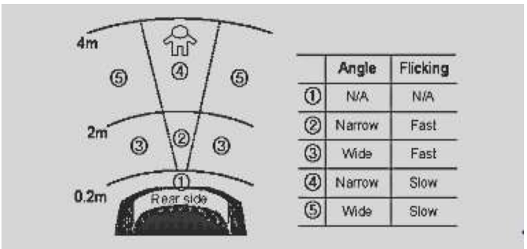

Fig. 21. Dynamic pattern control of the proposed on-road projection with an ultrasonic sensor based on the location of pedestrians.

Fig. 22. Projection angle control for LD1 and LD2. (a) Narrow and (b) wide.

In a vehicle as shown in Fig. 20. Depending on the location of pedestrians detected by the ultrasonic sensor, the projection angle and the flicking of laser patterns can be controlled as shown in Fig. 21. When pedestrians are too close to the rear bump around region 1 _, dynamic on-road projection is disabled for eye safety. The projection angle covers the location of pedestrians detected by an ultrasonic sensor. In order to warn pedestrian as the vehicle gets closer, the flicking of laser pattern becomes faster. Since an ultrasonic sensor can detect multiple points, the proposed system corresponds to the multiple pedestrians. Fig. 22 shows the two different angular control of the projected laser pattern without adjusting the duty-cycle to verify the maximum

Fig. 23. Implementation of the proposed on-road projection with an ultrasonic sensor.

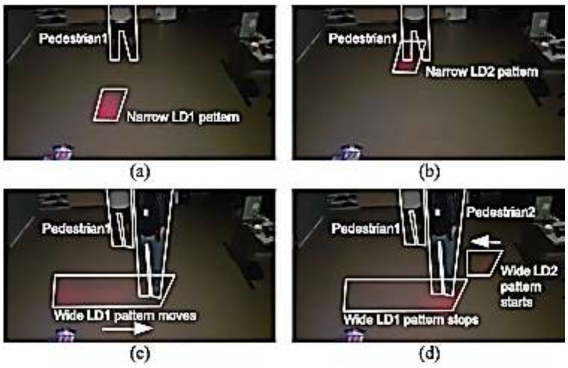

Fig. 24. Projected on-road real-time dynamic patternwith two LDs depending on the location of pedestrians: (a)(b) Pedestrian located 3m away from the sensor (pattern: narrow and slow) (c)(d) Pedestrian located 1.5m away from the sensor (pattern: wide and fast).

Projected angle of±70o at themaximum power of 0.98W,where VDD = 4.5 V, icoil = 200 mA VLD = VLD2 = 2.2 V, iLD1 = iLD2 = 18 mA, and B = 55 mT. The prototype is implemented as depicted in Fig. 23. Even though there are two MCUs for the prototype, one for the ultrasonic sensor and the other for
projection control, it can be integrated in a single MCU. Fig. 24 shows the projected real-time dynamic pattern corresponds to the control scheme in Fig. 21 depending on the location of pedestrians [32].

VI. CONCLUSION

In order to avoid collisions between vehicles and pedestrians, vehicle warning systems have been widely researched. This paper presents a vehicle warning system using dynamic patterns projected onto the road with a wide angle. In order to generate various dynamic patterns, an active mirror and laser diodes are controlled in terms of frequency and duty-cycle. The proposed system emits various dynamic patterns by using two laser diodes with emission angles up to ±70°. The proposed technique along with an ultrasonic sensor technology for pedestrian recognition generates dynamic patterns automatically projected depending on the position of pedestrians. In addition, the proposed active mirror in conjunction with a micro-electro mechanical system (MEMS) technology can be implemented in an area much smaller than the prototype.

REFERENCES

[1]. R. Retting and H. Rothenberg, "Pedestrian traffic fatalities by state: 2018 preliminary data," Governors Highway Safety Association, Washington, DC, USA, Feb. 2019. [Online]. Available: https://www.ghsa.org/sites/ default/files/2019-02/FINAL_Pedestrians19.pdf

[2]. "Traffic Safety Facts: 2016 Data," National Highway Traffic Safety Administration, Washington, DC, USA, Mar. 2018. [Online]. Available:https://crashstats.nhtsa.dot.gov/Api /Public/ViewPublication/812493

[3]. "Non-Traffic Surveillance: Fatality and Injury Statistics in Non-Traffic Crashes in 2015," National Highway Traffic Safety Administration, Washington, DC, USA, Apr. 2018. [Online]. Available: https://crashstats.nhtsa.dot.gov/Api/Public/ViewPublication/812515

[4]. P.-F. Ho and J.-C. Chen, "WiSafe: Wi-Fi pedestrian collision avoidance system," IEEE Trans. Veh. Technol., vol. 66, no. 6, pp. 4564–4578,Jun. 2017.

[5]. A. T.-Sarvestani, H. N. Mahjoub,Y. P. Fallah, E.M.-Pari, and O. Abuchaar, "Implementation and evaluation of a cooperative vehicle-to pedestrian safety application," IEEE Intell. Transp. Syst.Mag., vol. 9, no. 4, pp. 62–75, Winter 2017.

[6]. K. Abboud, H. Aboubakr Omar, andW. Zhuang, "Interworking of DSRC and cellular network technologies for V2X communications: A survey,"IEEE Trans. Veh. Technol., vol. 65, no. 12, pp. 9457–9470, Dec. 2016.

[7]. V. Goud and V. Padmaja, "Vehicle accident automatic detection and remote alarm device," Int. J. Reconfigurable Embedded Syst., vol. 1, no. 2, pp. 49–54, Jul. 2012.

[8]. J. G. Casali and K. Alali, "Vehicle backup alarm localization (or not): Effects of passive and electronic hearing protectors, ambient noise level,and backup alarm spectral content," in Proc. Human Factors Ergonomics Soc., 2009, pp. 1617–1621.

[9]. J. G. Casali, G. S. Robinson, E. C. Dabney, and D. Gauger, "Effect of electronic ANR and conventional hearing protectors on vehicle backup alarm detection in noise," Human Factors, vol. 46, pp. 1–10, 2004.

[10]. Mitsubishi Electric Corporation, For Immediate Release, no. 2970, 2015. [Online]. Available: http://www.mitsubishielectric.com/news/2015/1023.html

[11]. M. Suwa, M. Nishimura, and R. Sakata, "LED projection module enables a vehicle to communicate with pedestrians and other vehicles," in Proc.Int. Conf. IEEE Consum. Electron., Berlin, Germany, 2017, pp. 37–38.

[12]. S. Rizvi, M. Knöchelmann, P. Ley, and R. Lachmayer, "Survey of on-roadimage projection with pixel light systems," Proc. SPIE, vol. 10603, 2017,Art. no. 1060314.

[13]. A. Wolf, G. Kloppenburg, R. Danov, and R. Lachmayer, "DMD basedautomotive lighting unit," in Proc. DGaO,Aug. 2016, doi: 10.15488/4004.

[14]. G. Kloppenburg, A. Wolf, and R. Lachmayer, "High-resolution vehicleheadlamps: Technologies and scanning prototype," Adv. Opt. Techno.,vol. 5, no. 2, pp. 147–155, 2016.

[15]. A. Dancu et al., "Gesture bike: Examining projection surfaces and turnsignal systems for urban cycling," in Proc. Int. Conf. Interactive Tabletops Surf., 2015, pp. 151–159.

[16]. A. Dancu, Z. Franjcic and M. fjeld, "Smart flashlight: Map navigationusing a bike-mounted projector," in Proc. SIGCHI Conf. Human Factors Comput. Syst., Toronto, ON, Canada, 2014, pp. 3627–3630.

[17]. T. Zhao,X. Zhang,W. Mao, F.Wang, J. Xu, andY. Gu, "Amodified hybrid modulation strategy for suppressing DC voltage fluctuation of cascadedH-bridge photovoltaic inverter," IEEE Trans. Ind. Electron., vol. 65, no. 5,pp. 3932–3941, May. 2018.

[18]. J.-S. Lee, H.-W. Sim, J. Kim, and K.-B. Lee, “Combination analysisand switching method of a cascaded H-Bridge multilevel inverter based on transformers with the different turns ratio for increasing the voltagelevel,” IEEE Trans. Ind. Electron., vol. 65, no. 6, pp. 4454–4465,Jun. 2018.

[19]. D. Sha, G. Xu, and Y. Xu, “Utility direct interfaced charger/dischargeremploying unified voltage balance control for cascaded H-Bridge units anddecentralized control for CF-DAB modules,” IEEE Trans. Ind. Electron.,vol. 64, no. 10, pp. 7831–7841, Oct. 2017.

[20]. Y. Yu, G. Konstantinou, B. Hredzak, and V. G. Agelidis, “Operationof cascaded H-Bridge multilevel converters for large-scale photovoltaic power plants under bridge failures,” IEEE Trans. Ind. Electron., vol. 62,no. 11, pp. 7228–7236, Nov. 2015.

[21]. G. Farivar, B. Hredzak, and V. G. Agelidis, “Reduced-capacitance thinfilmH-bridge multilevel STATCOM control utilizing an analytic filtering scheme,” IEEE Trans. Ind. Electron., vol. 62, no. 10, pp. 6457–6468,Oct. 2015.

[22]. E. Babaei, S. Laali, and S. Alilu, “Cascaded multilevel inverter with seriesconnection of novel H-Bridge basic units,” IEEE Trans. Ind. Electron., vol. 61, no. 12, pp. 6664–6671, Dec. 2014.

[23]. P. Karamanakos, K. Pavlou, and S.Manias, “An enumeration-basedmodelpredictive control strategy for the cascaded H-bridge multilevel rectifier,” IEEE Trans. Ind. Electron., vol. 61, no. 7, pp. 3480–3489, Jul. 2014.

[24]. B. Gao, J. Xu, J. Zhao, and N. Xi, “Combined inverse kinematic and staticanalysis and optical design of a cable-driven mechanism with a spring spine,” Adv. Robot., vol. 26, no. 8-9, pp. 923–946, 2012.

[25]. B. Gao, H. Song, L. Sun, and Y. Tang, “Inverse kinematics and workspaceanalysis of a bio-inspired flexible parallel robot,” in Proc. Int. Conf. IEEE Cyber Technol. Autom., Control Intell. Syst., 2013, pp. 138–143.

[26]. B. Gao, J. Hu, S. Guo, W. Li, and Q. Kan, “Lateral bending models ofspring spine for cable-driven parallel mechanism,” in Proc. 11th World Congr. Intell. Control Autom., 2014, pp. 3176–3180.

[27]. L. Nagua, C. A. Monje, J. Muñoz, and C. Balaguer, “Design and performancevalidation of a cable-driven soft robotic neck,” presented at the Nat. Robot. Conf., Vallladolid, Spain, Jun. 12–14, 2018.

[28]. S.Timoshenko, Theory of Elastic Stability.NewYork,NY, USA: McGraw-Hill, 1963.

[29]. R. Frisch-Fay, Flexible Bars, London: Butterworths, 1962.

[30]. D. Halliday, J.Walker, and R. Resnick, Fundamental of Physics.Hoboken,NJ, USA: Wiley, 1960.

[31]. M. Sadiku, Elements of Electronics. New York, NY, USA: Oxford Univ.Press, 1989.

[32]. [Online]. Available: http://oasis.korea.ac.kr/ORP.mp4

[33]. On-Road Dynamic Pattern Projection Using an Active Mirror for Vehicle Warning Systems. IEEE TRANSACTIONS ON VEHICULAR TECHNOLOGY, VOL. 69, NO. 5, MAY 2020